# Extended (Bi-Modal) Ion Conics at High Altitudes

W.K. Peterson, H.L. Collin, M.F. Doherty[1] and C.M Bjorklund

*Lockheed Palo Alto Research Laboratory, Palo Alto, California*

Ion energization both parallel and transverse to the local magnetic field was observed on every crossing of the auroral zone by the Dynamics Explorer -1 Satellite. Not infrequently, ion distributions characterized by both significant parallel and transverse energization were found. These distributions have flux maxima over extended energy and angular ranges and were initially called bi-modal in the belief that they are the result of quasi-independent ion energization processes acting transversely and parallel to the local magnetic field. Recently it has been shown that some extended (bi-modal) ion distributions can be formed by mesoscale processes acting over an extended altitude range. Knowledge of the occurrence frequency and characteristics of extended ion distributions can be used to improve our understanding of the physical process responsible for their formation. We have developed and used an automated procedure based on standard image processing techniques to identify and characterize ion distributions that have been significantly energized transverse to the local magnetic field. Our survey found approximately 10,000 events in over 2,500 hours of data. We found about half of the $O^+$ and $He^+$ ion conic distributions identified had, in addition, a significant upward field-aligned component. Most of these extended ion conic distributions were found above 15,000 km, while the ion conic distributions with a restricted angular distribution and without a field-aligned component had an approximately uniform occurrence frequency over the altitude range from 8,000 to 24,000 km.

## INTRODUCTION

Ion conics are characterized by velocity space distributions with significant intensity maxima on a cone shaped surface centered on the magnetic field line direction. These strongly peaked angular distributions imply the existence of very intense and perhaps localized processes transferring energy to the ions. Investigation of the processes responsible for ion conic formation is required to understand the extraction and energization of low energy (~ 1 eV) ionospheric ions and their transport to the plasma sheet where they are quasi-isotropic and have energies on the order of 1 keV.

Two types of ion conic distribution have been identified in the plasma flowing upwards above the auroral and polar cap ionosphere. Sharp et al. [1977] and other investigators using data from the S3-3 satellite assumed that the peak flux in ion conic distributions was characterized by one cone angle for all energies. Such distributions could be created by the localized transfer of energy to a cool plasma. The S3-3 measurements available to Sharp et al. were limited to energies above 500 eV. The high sensitivity and low energy range of the DE -1 EICS instrument, [Shelley et al., 1981], allowed Klumpar et al. [1984] to identify a new class of conics characterized by an extended range of pitch angles. Klumpar et al. noted that this new class of ion conic distribution was also characterized by a significant maximum in flux of energetic ions aligned with the magnetic field. Klumpar et al. called these distributions bi-modal conics and attributed them to the occurrence of both transverse and parallel (to the local magnetic field) acceleration processes. Temerin [1986], Chang et al. [1986], and Horwitz [1986] have suggested alternative mechanisms for forming extended ion conic distributions.

[1]Present address: 913 Laguna Ave., Burlingame, California 94010

Space Plasmas: Coupling Between Small and Medium Scale Processes
Geophysical Monograph 86

Figure 1 shows examples of the two types of ion conic distribution displayed in the flux image format.

Progress in understanding ion conic formation has been limited by a lack of detailed examples, including fluxes and temperatures, of ion conics, especially the extended type. There have been several reports on the average proprieties of a large number of ion conics, but the data for these reports (e.g. Gorney et al. 1981; Thelin et al. 1990; Miyake et al. 1993) has come from visual examination of high time resolution images. The notable exception was the series of papers by Yau et al. [1984], Sagawa et al. [1987] and Kondo et al. [1990]. Yau introduced a one dimensional algorithm to search for peaks in the angular distribution over three broad energy ranges (0.01-1, 1-4, and 4-17 keV) and applied it to the high altitude data to identify ion conic events in three broad energy ranges. This classification technique was extended by Sagawa el al. [1987] and Kondo et al. [1990] to include other types of ion distributions, but these studies were also limited by the three broad energy ranges and were not able to provide much information about extended ion conics. Recently Miyake et al. [1993] have been able to distinguish between the two basic types of ion conic distributions in a large number of events. To date Miyake et al. have limited their studies to conic angular distributions of the restricted type.

To progress further in our understanding of the processes responsible for ion conic formation we need to determine the relative importance of the types of conic distribution in various regions of the magnetosphere. Such information on conic type and related energy and angular characteristics can only come from detailed evaluation of the characteristics of thousands of ion conic distributions. To meet this need, we have developed a two-dimensional, model-based algorithm to identify and classify energetic ion conic events in the plasma flowing upward on auroral and polar cap field lines. Our model-based algorithm is based on casting observed ion distributions into two dimensional flux images and applying standard image processing techniques [Doherty et al., 1993]. Using our algorithm it is possible to classify and characterize a large number of ion conic events and to determine the relative importance of the bi-modal (extended) conics identified by Klumpar et al. [1984]. Our model and method are novel, and it is impractical to physically check the specific identification of each distribution. We will therefore not characterize ion distributions as bi-modal, rather we will characterize them as either restricted or extended.

The rest of this paper is organized as follows. We first discuss the large (over 100,000 samples) data base of flux images we have assembled and the model-based algorithm. We then present results of the application of our algorithm to

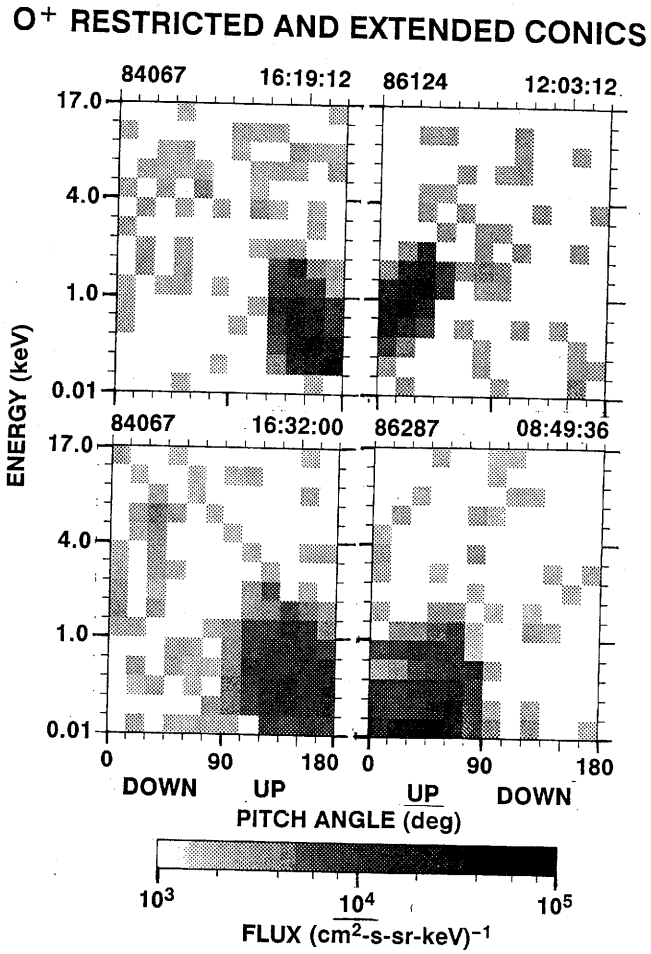


Fig. 1. Flux images of four oxygen ion conic distributions. The top two images are conic distributions with extended angular distributions. The bottom two images show distributions classified as having restricted angular distributions by the algorithm discussed in the text. Each image consists of a 15 × 12 pixel array where the oxygen ion flux intensity is encoded using the gray bar at the bottom. The energy/pitch angle sampling space is covered in 15 energy bands (ordinate) and 12 pitch angle bins (abscissa). The lowest energy band covers the range from 10 eV to ~ 100 eV. Successive energy bands are are quasi logarithmically spaced in energy over the range to 17 keV. The pitch angle range extends from 0° to 180°. Pitch angle is defined as the angle between the ion velocity and the local magnetic field. In the northern (southern) geomagnetic hemisphere 0° (180°) pitch angles correspond to ions flowing downward toward the ionosphere. The two images on left (right) were acquired in the northern (southern) geomagnetic hemisphere. The direction of ion flow is indicated on the respective pitch angle axes. Conic distributions have the most intense fluxes at pitch angles not aligned with the local magnetic field. The time that each image was acquired is indicated at the top of each image. For example the top right image was acquired at 16:19:12 universal time on the 67th day of 1984 (March 7).

the data base and make some observations about the distribution in space of transverse ion energization processes.

## THE DATA BASE OF FLUX IMAGES

The data we are working with come from the Energetic Ion Composition Spectrometer (EICS) on the Dynamics Explorer (DE) -1 Satellite. The DE program has been described by Hoffman and Schmerling [1981], and the EICS instrument by Shelley et al. [1981]. Briefly DE -1 was launched in August 1981 and operated until February 1991 in a 23,500 x 550 km, 90° inclination orbit. The data used this report were restricted to those acquired above 8,000 km and at invariant latitudes greater than 58°. The EICS instrument returns measurements of the ambient, mass-resolved ion fluxes in the energy range from spacecraft potential to 17 keV/e. The complete range of ion pitch angles was sampled twice per spacecraft spin period, six seconds. Since the count rate from only one mass/energy/angle value was available during each measurement interval (1/32 s), the sequence of mass and energy steps scanned was programmable. The most commonly used modes covered the energy range from 10 eV/e to 17 keV/e in 15 logarithmically spaced steps. Mass information was obtained in three fundamentally different modes: Mass scan, drum and fast modes which are characterized by instrument cycle times of 128, 96 and 24 seconds respectively. Data transmitted to the ground was processed and inserted into two distinct data bases.

The high resolution data base contains all of the data acquired for all modes. Peterson et al. [1988] have presented examples of ion conic events found in the high resolution data base. The summary data base is assembled from the sub-set of the high resolution data obtained in the drum and fast modes for three of the major ion species ($H^+$, $He^+$ and $O^+$). The summary data base is composed of ion fluxes binned in energy and pitch angle and averaged over successive 96 second intervals. Approximately half of the ~ 40,000 hours of DE -1 EICS data acquired were captured in the high resolution data base before the NASA computer center processing them was shut down in 1991. Most (~90%) of these high resolution data were acquired in the drum or fast modes and inserted into the summary data base. Approximately half of the summary data have been transferred to a 12 inch worm optical disk system using NASA supplied hardware and software [Davis and Vaidta, 1989]. Because mounting tapes is so labor intensive we have elected to use the part of the summary data base resident on optical disk for this study. The ~10,000 hours of summary data on the optical platter represent approximately 1/4 of all DE -1 EICS data acquired.

The model based algorithm described in the next section uses ion data in the form of "flux images". A flux image is constructed for each ion species and each 96 s interval. It consists of a pitch angle/energy space with pitch angle divided into 12 bands each of 15° width, and 15 energy levels spaced quasi-logarithmically from 0.01 to 17 keV. Thus the space is partitioned into a matrix of 12 x 15 pixels. Each pixel contains the ion flux obtained from the summary data base for the corresponding energy and pitch angle. These fluxes form a surface in pitch angle/energy space which is an image of the ion distribution. Figures 1-10, described below, are examples of flux images. Associated with each flux image is an identically partitioned matrix of 12 x 15 pixels which contains the standard deviations ($\sigma$) of the corresponding fluxes and forms an "error image". The standard deviations are also obtained from the summary data base and are estimated on the basis of Poisson counting statistics only.

## THE ALGORITHMIC MODEL OF CONICS

The algorithm examines data from each ion species in each 96 s interval in turn and searches for conics which are moving either parallel or antiparallel to the magnetic field direction. The field direction is downward towards the Earth in the northern geomagnetic hemisphere and upward away from the Earth in the southern hemisphere. Since the summary data base includes the geomagnetic latitude, the direction of the conic, upward or downward, can also be determined. If any conics are identified, a description of each is retained to from a data base of conics for further analysis.

Our first attempts to automatically identify conics in flux images were based on calculating one-dimensional properties of the image: the flux weighted pitch angle averaged over all energies, and the angular width of the angular peak in pitch angle at half the maximum flux intensity, averaged over all energies. This algorithm was not very sensitive to the differences between ion conic distributions extended in angle and trapped ion distributions because both distributions are characterized by a relatively large angular width. We found that extended and trapped ion distributions can be distinguished if the algorithm is extended to two dimensions (energy and angle).

The two-dimensional, model-based algorithm described here uses standard image processing techniques to process each flux image and the associated error image. In the flux image a conic forms a ridge running from low to high energy. A line along the length of the ridge is the conic path. Our algorithm identifies this conic path. In this respect it is identical to the way ion conics are visually identified on high resolution contour plots. The model requires that the following conditions hold true for a flux image to be identified as a

conic:

1. Conics have a pitch angle specificity; thus, within any particular energy level, the distribution has a well-defined maximum;

2. Conics span at least three energy levels;

3. The conic path remains at a constant pitch angle or steadily moves away from the central (i.e. 90°) pitch angle as energy decreases;

4. Conic paths include pitch angles either completely less than 90° or completely greater than 90°. This requirement separates conic distributions into those flowing up and down magnetic field lines.

In addition to the above attributes or rules used to identify conics, it was discovered in the course of testing our algorithm that we needed to identify ion beams and trapped ion distributions, which were sometimes mistaken for conics, in order to minimize the number of false positive ion conic detections. Ion beams in the flux images input to our algorithm are characterized by a maximum flux level within a compact energy range and with a pitch angle range centered on the magnetic field direction. Figure 2 shows an example of an ion beam in the flux image format. Trapped ion distributions in flux image format have a high degree of symmetry about 90° pitch angle as shown in Figure 3.

Two characteristics of the data in the lowest energy channel complicate its use in the analysis and characterization of ion conic events. For oxygen ions the energy range of the lowest energy channel (10 eV to 100 eV) sometimes contains a contribution from a low (~ eV) energy cold rammed oxygen plasma which introduces an additional angular maximum. In addition, the broad energy width makes it extremely difficult to determine the average energy of the flux in the lowest energy channel. It is probable that the model-based algorithm we have developed to identify ion conic distributions can be extended to include data from the lowest energy channel. For the present study, however, we have restricted our interest to the highest 14 energy channels covering the energy range 150 eV to 17 keV.

Our algorithm has four stages: image formation, image compression, pixel qualification and conic path evaluation. The following paragraphs provide further detail on each of these stages.

*Image formation.*

A large number (roughly 50%) of the 96 second intervals included in the summary database were obtained in regions with little or no measurable ion flux. It is desirable to reliably identify empty flux images, reject them from further investi-

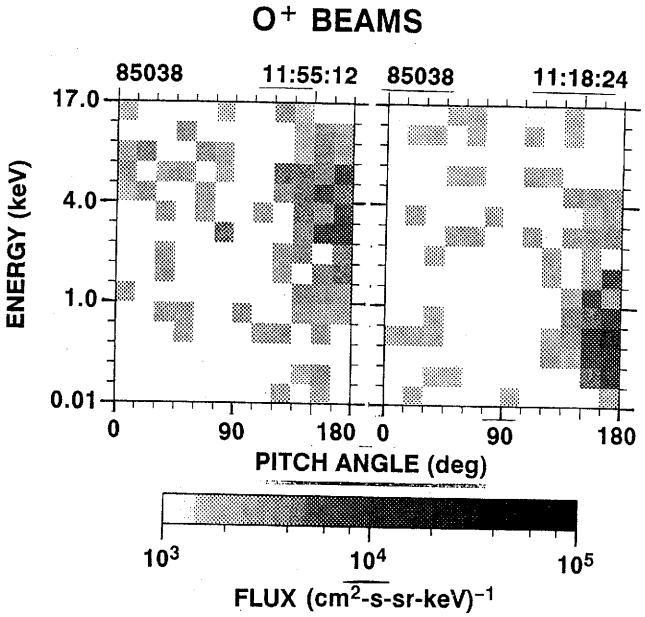


Fig. 2. Flux image of two oxygen ion beam distributions in the same format as Figure 1. The most intense fluxes in the ion beams occur along the magnetic field direction. The ion beam is further characterized by a more compact extent in energy and pitch angle. Note that the energy and particularly the angular resolution of the ion flux measurements place limits on the experimental differentiation between ion beams and ion conic distributions. In particular, restricted ion conics with a conic angle less than 15° will be characterized as ion beams. The examples in Figure two were both acquired in the northern geomagnetic hemisphere.

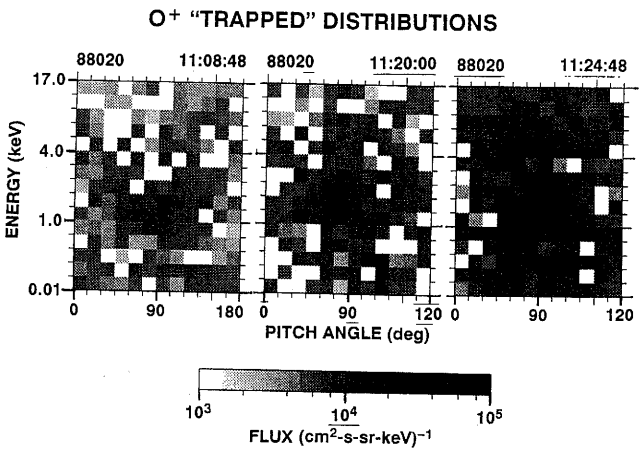


Fig. 3. Flux images of three oxygen ion trapped distributions in the same format as Figure 1. Note the symmetry about the 90° pitch angle axis.

gation, and to set a repeatable flux threshold for the detection of ion conic distributions. As noted above the data for each mass in each 96 second interval consist of a pair of a flux image and the corresponding error image containing ion fluxes and estimates of the standard deviations ($\sigma$) of the fluxes. Our algorithm requires that a minimum number of flux values in the flux image have magnitudes greater than the estimate of their standard deviation. The minimum number was set based on examination of the training results, and is specific to each mass type: 10 pixels for $H^+$, 7 for $O^+$, and 4 for $He^+$. This pre-selection considerably speeds up processing but is set low enough that it does not reject any conic distributions.

*Image compression.*

The flux images are next processed to remove certain energy bands from consideration, thus relieving the more computationally intensive qualification and evaluation stages of the algorithm. An energy band is declared valid if there exists some difference (i.e. angular dependence) in the scaled flux pixel values within that band. Homogeneous bands are assumed to indicate isotropic distributions or background noise and are ignored. (To discriminate against ion beams, flux values at pitch angles of 0° and 180° are not considered when performing this check.) A second test checks to see if the maximum flux value for a band exceeds a minimum threshold. (Again, flux values at the two outer pitch angles are ignored.) The minimum threshold value is set to the expected 1-$\sigma$ value of the background noise of the flux measurements. This test ensures that a few pixels which exceed one standard deviation in their flux values do not adversely affect the algorithm performance. Finally, the largest flux value over all energy bands and pitch angles is compared with a pre-set minimum (chosen from a manual review of the training data set described below) for each possible ion type. If this value is not exceeded, the flux image is dropped from further processing.

Image compression is completed by eliminating the highest energy bands. Starting from the lowest energy, each energy band is checked for validity. If two adjacent energy bands are invalid, then those two bands and the remaining bands of higher energy levels are eliminated from further consideration. Subsequent processing uses this compressed image which can contain up to fourteen contiguous energy bands.

*Pixel qualification.*

For each flux pixel in the compressed image, a comparison is made between it and its standard deviation value ($\sigma$) from the error image. If the flux value exceeds the standard deviation, the pixel is marked as a candidate for inclusion in a conic structure. Figure 4 presents graphically the results of the pixel qualification test applied to the $O^+$ flux image obtained at 16:32 on March 7, 1984 shown in Figure 1

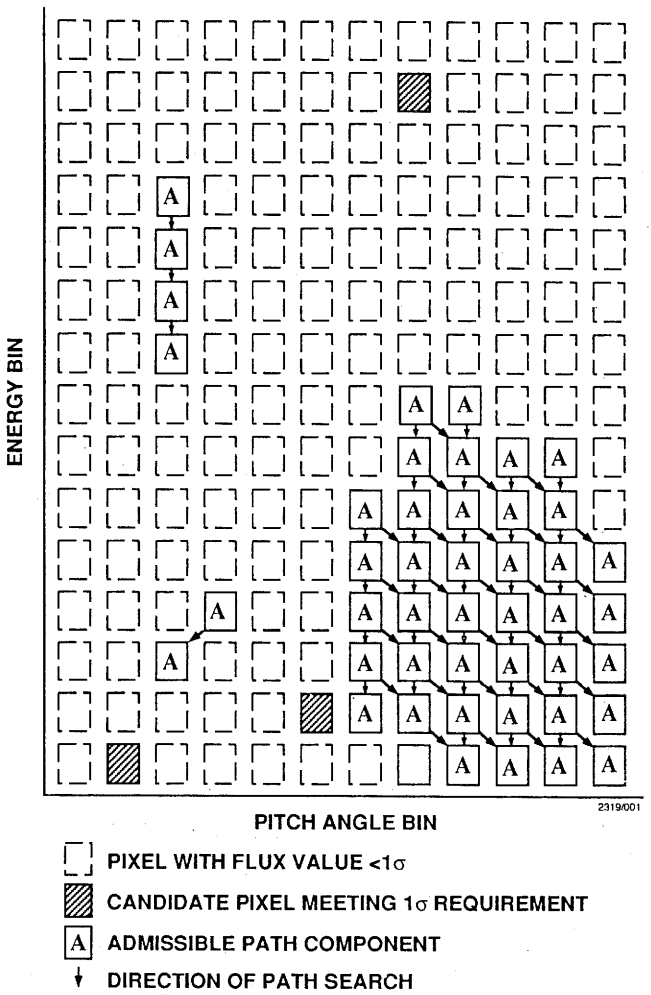


Fig. 4. Analysis of the conic path. See text for details.

.An additional qualification check eliminates trapped ion distributions. Our algorithm checks for trapped ion distributions at this stage by calculating the ratio of the number of symmetric (about the 90° pitch angle) pairs of candidate conic pixels within each energy band level. If the ratio of symmetric pairs of candidate pixels to total candidate pixels exceeds 70%, then the image is declared to be of a trapped ion distribution, and no further processing is done.

*Conic path evaluation.*

Our model requires that the conic path in energy/pitch angle

space remains at a constant pitch angle or steadily moves away from the central (90°) pitch angle as energy decreases. The algorithm creates tree structures, consistent with this requirement, of the candidate pixels which passed the qualification step above. A recursive search of these tree structures is performed and a set of candidate paths identified. Each path must also extend at least 3 energy levels. Compare the diagram in Figure 4 with the conic image in the lower left of Figure 1; the pixels which qualify have been pictorially represented in Figure 4, with the possible path routes highlighted with arrows. Since there are several possible paths which can be selected through the candidate pixels for any one conic event, we have defined a merit function to select the best path based on quantifiable measurements. This function also yields a relative perspective as to how certain our algorithm is that any one event is, or is not, a conic event. We have evaluated two merit functions: M1) a simple sum of the flux magnitudes for all pixels in a path; and M2) a numerical integral of the velocity space density along the conic path. M2, is obtained by summing the velocity space density elements at a given energy and pitch angle $f(E,\theta)$ which is proportional to the measured flux intensity divided by the energy of the measurement. The merit function M2 takes into account the variable width of the energy bins. In sample runs, merit function M2 selected conic paths that were deemed more reasonable for conic distributions extending over a large energy range than did M1. We have accordingly used M2 to identify conic paths in the results presented below.

The merit function indicates the relative heights of the candidate paths running along the ridge formed by the conic in its flux image. By maximizing the merit function, the path running closest to the apex of the ridge is identified. All candidate paths are evaluated. The path which has the maximum merit function value is saved as part of the description of the conic and is reported to the end-user if a conic is found in the flux image. For every conic event, we also record and save the value of the merit function of the conic path with the highest figure of merit flowing in the opposite direction. Figure 5 shows an $O^+$ conic distribution with several distinct candidate paths on the left and the conic path with the largest figure of merit indicated on the right. At this point the algorithm has tentatively identified a candidate ion conic. In our training experiments, however, we observed that there were still large numbers of false positive detections due to confusion with another type of ion distribution ---- asymmetric counter streaming ion conics. Dual conic distributions or asymmetric counter streaming ion conics, are a common feature in the data as reported by Sagawa et al. [1987]. These appear to be a separate phenomenon from the restricted and extended types of conic and are rejected by the algorithm described here. Dual conic distributions exist when candidate

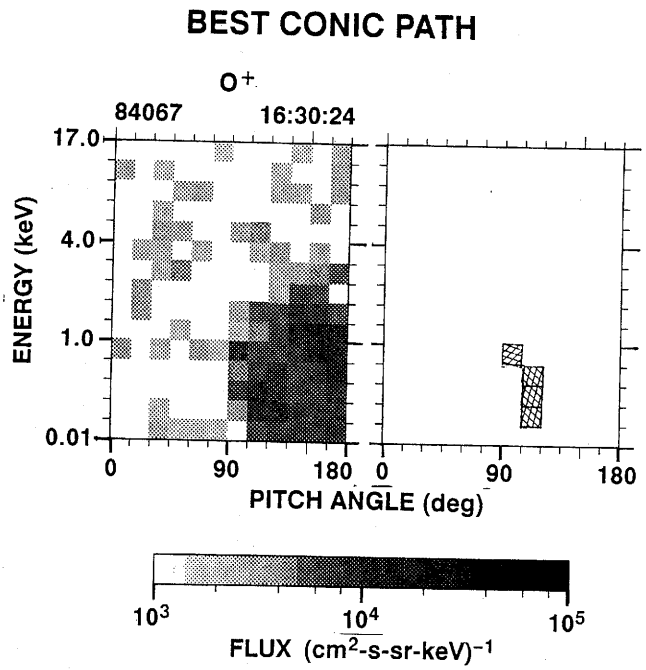


Fig. 5. Left: Oxygen ion flux image in the same format as Figure 1. Right: The conic path with the highest figure of merit identified by our algorithm is highlighted. This path identifies the flux image as that of a restricted conic distribution. The data in Figure 5 were acquired in the northern geomagnetic hemisphere.

conics are found flowing in both the upward and downward directions. These distributions resemble trapped distributions with the additional feature of a flux minimum at 90°. Additional checks are made to exclude counter streaming conic distributions from the results:

1) A comparison between the figures of merit (defined above) corresponding to both halves of counter streaming conics is made. Specifically, if the smaller figure of merit is greater than 10% of the average of the two figures of merit, we do not classify the distribution as conic.

2) If the lengths of the conic paths are small (i.e. less than 5 pixels), then a symmetry test is performed (as described in the qualification stage) over just those energy bands in included in the candidate conic paths. These highly symmetric small conics are also rejected.

*Identification of restricted and extended ion conic distributions*

Extended and restricted conic distributions are distinguished by their conic paths. The conic paths for extended

distributions have their low energy pixel in the field aligned direction (pitch angles of 0° or 180°), and extend over at least 45° of pitch angle. The conic path for a restricted conic distribution terminates at the lowest energy used in the study and traverses at most 30° of pitch angle. Figures 6, 7, and 8, illustrate the way conic distributions are identified from the end points of the conic path. The conic path for the oxygen distribution in Figure 6 is characterized by a constant pitch angle and ends at the lowest energy included in the evaluation of conic paths (i.e. the second energy step). This is the type of conic distribution described by Sharp et al. [1977], which we term the restricted type. The conic path for the oxygen distribution in Figure 7 is characterized by a range of pitch angles terminating in a pixel in the magnetic field direction. This type of conic distribution was first described by Klumpar et al. [1984], and is termed the extended type. Figure 8 shows a candidate conic path that does not terminate at pixels either at the lowest energy or in the magnetic field direction. We do not consider images such as that shown in Figure 8 to be of an ion conic.

## TESTING THE ALGORITHM

The results of the supervised runs on the 400 training set events showed that we regularly identified all of the conic events and rejected all of the trapped ion events. The algorithm also identified as conics a small number of downflowing conic events, and was not capable of identifying ion conics in the presence of a large quasi-isotropic background ion flux. These anomalies are addressed below.

Figure 9 shows an interval where $O^+$ and $He^+$ conics were found, but where an intense, quasi-isotropic flux of $H^+$ ions obscured detection of an $H^+$ conic distribution. It would be possible to modify the algorithm to systematically subtract an isotropic flux from the observed distributions before searching for ion conic distributions. Because all of the $O^+$ and $He^+$ ion conic distributions found in the training set did not have a quasi-isotropic distribution obscuring the ion conic distribution, and because information on the energy and flux distributions of oxygen and helium ion conic distributions are of current interest, we elected to use the algorithm as described above, and restrict our initial investigations to $O^+$ and $He^+$ ion conic distributions. It is interesting to note that the general presence of the $H^+$ background isotropic flux with energetic ion conic events was not expected prior to commencement of this study.

Figure 10 shows examples of hydrogen, oxygen, and helium distributions that are identified as downflowing conics by our algorithm. Specifically our algorithm found that the can-

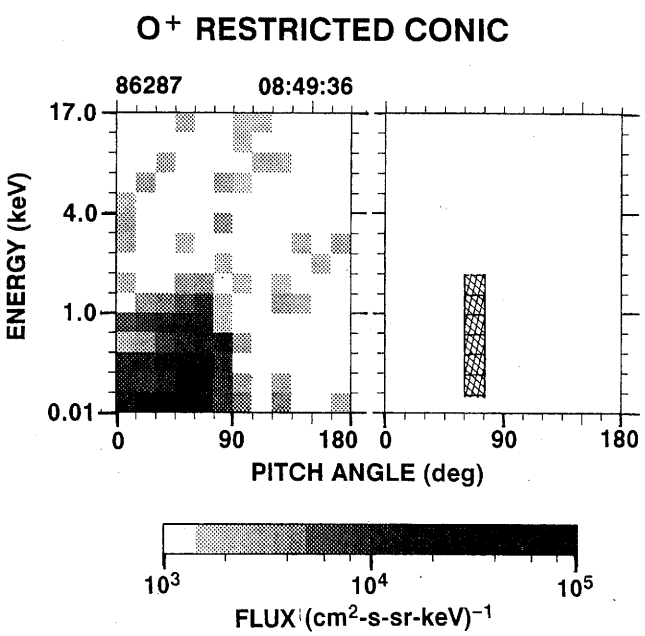


Fig. 6. Flux image of an oxygen restricted ion conic distribution in the format of Figure 5. The flux image was acquired in the southern geomagnetic hemisphere. Note that the conic path identified by our algorithm ends at the second energy channel, the lowest energy channel considered in this investigation.

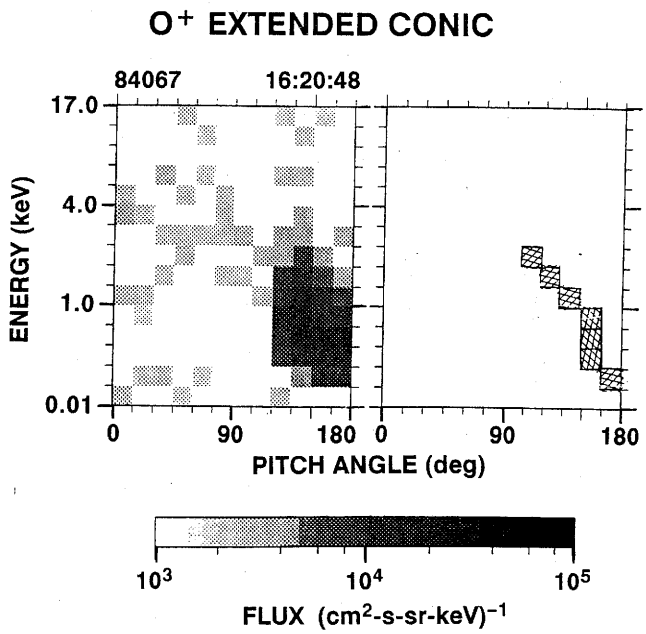


Fig. 7. Flux image of an oxygen extended ion conic distribution in the format of Figure 5. The data were acquired in the northern geomagnetic hemisphere. Note that the low energy end of the conic path is in the magnetic field direction (180° pitch angle).

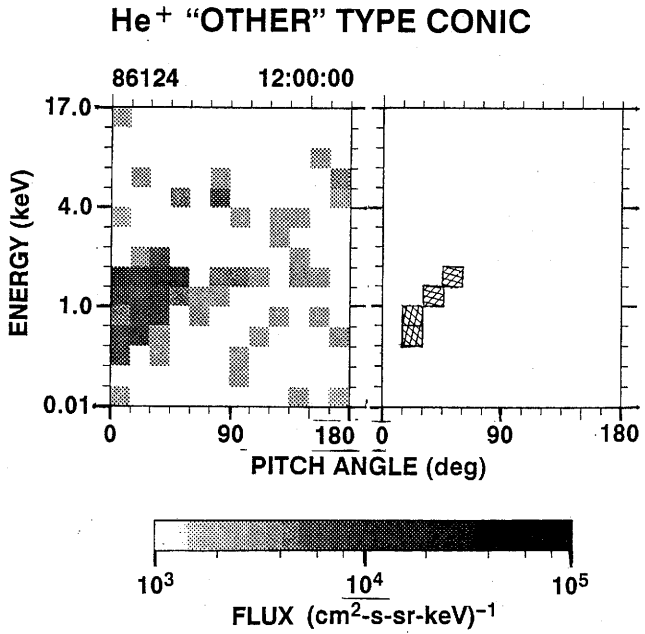


Fig. 8. Flux image of a helium ion distribution in the format of Figure 5. Here the identified conic path identified by our algorithm does not end in a pixel aligned with the magnetic field, or in the lowest energy channel considered. These distributions are not identified as conic distributions by our algorithm.

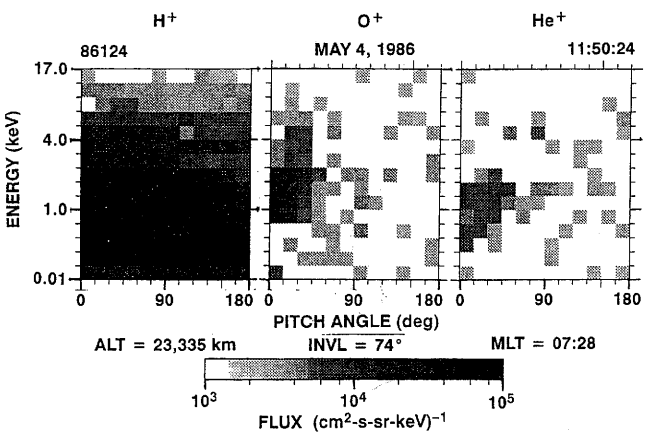


Fig. 9. Flux images of hydrogen, oxygen, and helium ion distributions acquired at 11:50:24 universal time on May 4, 1986 (i.e. day 124 of 1986) in the format of Figure 1. Our algorithm identified restricted oxygen and helium conic distributions. The intense, quasi-isotropic, flux of hydrogen ions obscured detection of any hydrogen conic distribution at this time.

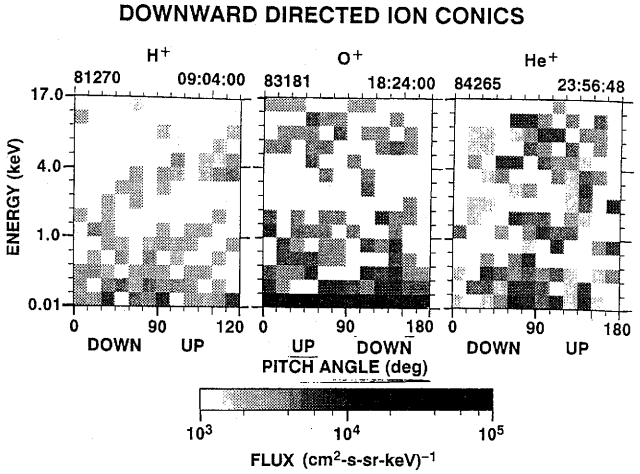


Fig. 10. Flux images of hydrogen, oxygen, and helium ion distributions where our algorithm identified downflowing, restricted, ion conics. The distributions were not acquired simultaneously. The hydrogen and helium distributions were acquired in the northern geomagnetic hemisphere and the oxygen was acquired in the southern. The direction of flow is indicated below the pitch angle axes (abscissa).

didate conic path with the highest figure of merit was characterized by pitch angles directing it downward into the ionosphere. Downward flowing ion conic distributions, if they exist at all, are rare and are restricted to pitch angles near 90°. See, for example, Gorney et al. [1985]. A large fraction of these downward flowing events identified by our algorithm were investigated. All downflowing events investigated were characterized by low flux levels and/or high background counting rates. We concluded that these were all false positive identifications. False positive identifications flowing up the field line were visually located in sample data runs after downward directed false positives were found. We could eliminate these upward false positive identifications by raising the threshold of detection but this would reduce the value of a survey because it would be restricted to only the most intense events. Instead we elected to make use of the downward false positives. The algorithm can be expected to make the same frequency of false identifications in both directions. We therefore can use the occurrence frequency of downward false positives as a measure of the frequency of occurrence of upward false positives and use this measure to correct the results. The occurrence frequencies reported below were calculated from the difference between the detected upward directed conics (including false positive) and downward directed false positives.

## APPLICATION OF THE ALGORITHM TO THE DATA BASE

Table 1 summarizes the results from the application of the algorithm to 122,390 $O^+$ and 67,100 $He^+$ flux images. As noted above the data base is restricted to energies above ~150 eV, acquired between September 1981 and April 1988 at altitudes between 8,000 and 24,000 km, invariant latitudes above 56° and all local times. Table 1 presents the occurrence frequency of restricted and extended conics in the sample data set. It shows that about 3 times more $O^+$ conics than $He^+$ are found, and that the ratio of restricted to extended type conics is about the same for both species (~ 3:2 ). An examination of the ion conic events shows that they have a flux threshold, referenced to 1000 km altitude, of ~ $10^4$ $(cm^2\text{-s-sr-keV})^{-1}$ and characteristic energy threshold of ~ 200 eV, a typical flux of > $10^6$ $(cm^2\text{-s-sr-keV})^{-1}$ and a typical characteristic energy of ~ 700 eV. These average results are representative of conics observed at apogee where most of the data were acquired. Figure 11 shows the distribution in altitude, invariant latitude, and magnetic local time of the 122,390 $O^+$ and 67,100 $He^+$ flux images searched. Figure 11 shows that, in general, the sampling in invariant latitude and magnetic local time was uniform. No samples are shown for invariant latitudes above 85°, because data acquired at high latitudes was treated as if it was obtained at 84° invariant latitude. Note that there are relative maxima in the number of samples at 64° invariant latitude and 14:00 magnetic local time. The average conic in Table 1 was detected at ~ 20,000 km and an invariant latitude (INVL) of ~ 70°, not where the average data interval was acquired. To proceed further we need to look at the occurrence frequency of ion conic events by species and type in the altitude, invariant latitude, and magnetic local time range sampled by the DE -1 satellite.

Figure 12 presents the frequency of occurrence as a function of altitude, invariant latitude (INVL) and magnetic local time (MLT) of the conic events listed in Table 1. $O^+$ and $He^+$ restricted and extended ion conics have similar MLT and INVL occurrence frequencies; the altitude dependencies are different. $He^+$ restricted and extended conic distributions have approximately the same occurrence frequency over the full altitude range (8,000 to 24,000 km), but the occurrence frequency of $He^+$ restricted conics increases slightly above ~15,000 km. $O^+$ restricted conic distributions show a larger increase in occurrence frequency above ~15,000 km than do the $He^+$ restricted conics. The occurrence of $O^+$ extended conics has the largest variation with altitude, increasing from $\leq$ 1.5% at 15,000 km to $\geq$ 3.5% at the highest altitudes sampled.

Energetic ion conics are found most frequently on the morning side of the magnetosphere between 06:00 and 13:00 MLT. There are also slight but systematic differences in the MLT distribution of the two types of conic events for both $O^+$ and $He^+$ identified by our algorithm. The $O^+$ conics, both

TABLE 1. Conics Found by Species and Type

| | $O^+$ | | $He^+$ | |
|---|---|---|---|---|
| Type: | Restricted | Extended | Restricted | Extended |
| UP | | | | |
| | 4,149 | 2,070 | 1,469 | 506 |
| | 3.39% | 1.69% | 2.20% | 0.75% |
| DOWN | | | | |
| | 818 | 131 | 849 | 129 |
| | 0.67% | 0.11% | 1.27% | 0.19% |
| NET | | | | |
| | 2.72% | 1.58% | 0.92% | 0.56% |

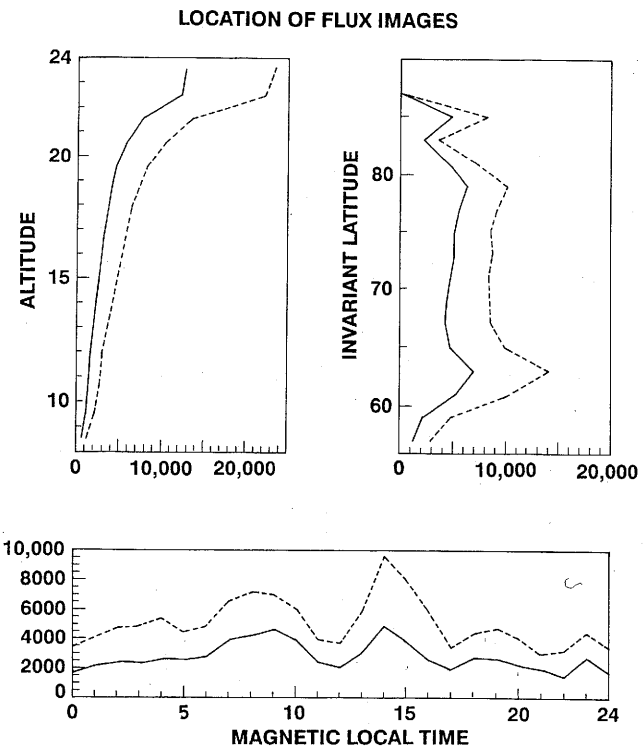


Fig. 11. Distribution of flux images examined in: 1,000 km altitude bins (top right), 2° invariant latitude bins (top left), and 1 hour magnetic local time bins (bottom) The distribution of oxygen flux images is indicated by the dotted lines and helium flux images by the solid lines. A total of 122,390 oxygen and 67,100 helium flux images are included in the data base used for this investigation.

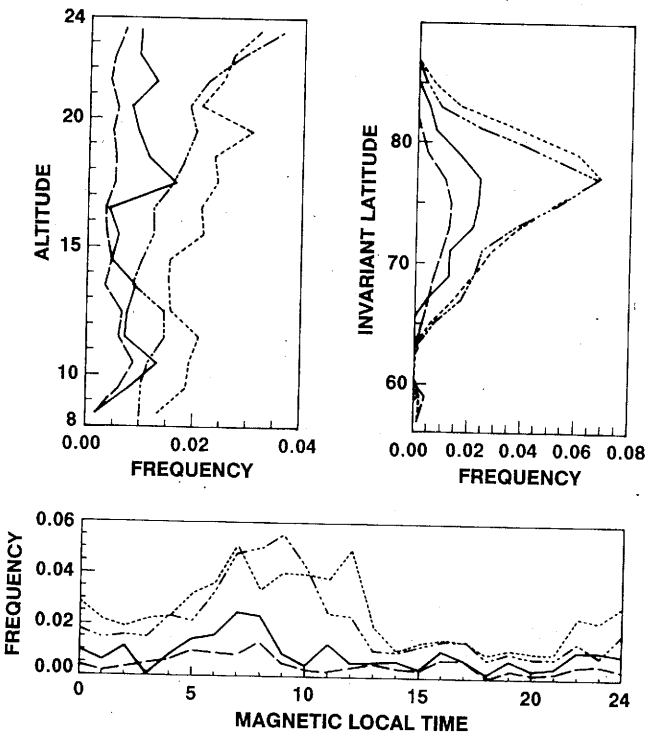


Fig. 12. Distribution in altitude (top left), invariant latitude (top right) and magnetic local time (bottom) of the corrected occurrence frequency of the four types of ion conic distribution identified by our algorithm. Key: ... $O^+$ restricted; _ .. _ $O^+$ extended; ____ He+ restricted; and _ _ _ $He^+$ extended.

restricted and extended, occur over a broader range of MLT than the $He^+$ conics. There is an increased occurrence frequency of both types of conics for both species starting at ~06:00 MLT and extending to ~13:00 MLT for $O^+$ restricted conics and earlier MLTs for restricted and extended $He^+$ conics. We also note that the pre-noon maximum in occurrence frequency is noticeably less for $He^+$ extended conic distributions.

Energetic ion conics identified by our algorithm are found most frequently above 70° INVL. $O^+$ conics occur poleward of $He^+$ conics, and the peak occurrence frequency of $He^+$ conics extends over a broader range of invariant latitude. There is also a very small poleward shift of extended conic distributions.

The results reported for the occurrence distribution of restricted ion conics in Table 1 and Figure 12 are mostly consistent with previous morphological studies. Because we have used a different technique to identify ion conics, we expect the present results to differ from those reported by Yau et al. [1984], Sagawa et al. [1987], and Kondo et al. [1990] which were also based on data from the DE -1 EICS instrument,but which were more coarsely binned in energy and angle. These authors used a one dimensional algorithm that identified angular peaks in three broad energy ranges. (10 eV - 1 keV, 1-4 keV, and 4-17 keV) for $H^+$ and $O^+$ ions. For $O^+$ Yau et al. [1984] found high occurrence frequencies (~20%) in the 10 eV - 1 keV energy channel, and frequencies comparable to those reported in Figure 12 in the higher energy channels. They found an altitude dependence for $O^+$ conics in the two high energy ranges similar to that of $O^+$ restricted conics shown in Figure 12. The Yau et al. $O^+$ invariant latitude distributions showed two relative maxima near 65° and 75°, compared to Figure 12 which shows a single maximum for $O^+$ conic occurrence above 75°. This difference arises from the different model dependent definitions of an ion conic distribution. In the present study we require that the figure of merit (defined above) of an ion conic distribution be at least 10 times that of any candidate conic distribution flowing in the opposite direction. The second, low latitude, maxima in conic occurrence frequency found by Yau et al. comes from the characterization of asymmetric counter streaming ion conic distributions noted by Sagawa et al. [1987] as ion conic distributions. The 6-12 MLT maxima and 15-20 MLT minima in $O^+$ restricted conic occurrence shown in Figure 12, are also clearly defined in the Kondo et al. [1990] results. Dayside maxima in ion conic occurrence has also been reported by Gorney et al. [1981], Thelin et al. [1990] and Miyake et al. [1993].

A side benefit of the identification of a conic path is the ability to take the flux values actually measured in each energy angle pixel along the path, $j(E,\theta)$, and use them to calculate characteristic fluxes and energies. We can then calculate average characteristic energies and fluxes and the variation of these average quantities over the altitude, invariant latitude and magnetic local time ranges available to us to provide further insight into the processes responsible for conic formation. There are many different quantities that we can calculate to characterize the flux and energy of ion conic events. Among them are the upward directed flux calculated using the measured fluxes in each pixel of the conic path, $J_{PATH}$, the flux weighted average energy associated with pixels in the conic path, $E_{PATH}$, and the net flux above the energy threshold used in our study, $J_{NET}$. These quantities are explicitly defined in equations 1-3.

$$J_{PATH} = \int_{PATH} \mathbf{j} \bullet \mathbf{n}\, dE \qquad (1)$$

$$E_{PATH} = \int_{PATH} E\, \mathbf{j} \bullet \mathbf{n}\, dE \;/\; J_{PATH} \qquad (2)$$

$$J_{NET} = \int_{LC}^{180} \int_{150\ eV}^{17\ keV} \mathbf{j} \bullet \mathbf{n}\, dE\, d\Omega \qquad (3)$$

Where **j** • **n** is the vector product of the directed flux and a unit vector in the magnetic field direction. The flux values used in equations 1-3 have all been normalized to 1,000 km using a dipole magnetic field model. The path in Equations 1 and 2 includes only flux pixels in the conic path determined by the algorithm described above. In Equation 3 the integral is taken over all energies and angles excluding those angles in the loss cone and those energies below the threshold used in this study, 150 eV. The velocity space density in pixels along the conic path $f(E,\theta) \propto j(E,\theta) / E$. It is therefore possible to define a temperature (kT in keV) by fitting a Maxwellian to the measured velocity space densities along the conic path

$$f(E) = \chi\ e^{-E/kT} \qquad (4)$$

In equation 4, $\chi$ and kT are the two constants determined from the fit of the velocity space densities $f(E_i, \theta_i)$ at the pixels located at energy and angle points $E_i$ and $\theta_i$ along the conic path. Evaluation of the average values of the quantities defined in equations 1-4 from the thousands of conic events identified by our algorithm also requires making a correction for the false positive conic events discussed above. In this report we will present results for $J_{PATH}$ and $E_{PATH}$. Presentation and discussion of the average values of $J_{NET}$, kT, and other quantities determined from the flux images and fluxes along the conic paths requires more space than is available here.

Figure 13 presents the average value of $J_{PATH}$ normalized to 1,000 km in units of $(cm^2\text{-s-sr-keV})^{-1}$ as a function of altitude, invariant latitude and magnetic local time. The average values plotted in Figure 13 have been corrected for the contribution of false positive conics by using the value determined from the identified, false positive, downflowing conics using the relation:

$$J_{PATH}(\Psi) \equiv \{N_U(\Psi) \times J_{UPATH}(\Psi) - N_D(\Psi) \times J_{DPATH}(\Psi)\} \div \{N_U(\Psi) - N_D(\Psi)\} \qquad (5)$$

Where $\Psi$ refers to one of the intervals of altitude, INVL, or MLT in Figure 13, N is the total number of conic events found in the interval $\psi$, $J_{PATH}(\psi)$ is the average value in that interval, and the subscripts U and D refer to upward and downward directed conics identified by the algorithm. $J_{PATH}$ values for $O^+$ restricted and extended conics and $He^+$ restricted conics are shown in Figure 13. $J_{PATH}$ for $He^+$ extended conics and all conics at invariant latitudes greater than 80° or less than 65° have been omitted from Figure 13, because the statistical uncertainty in their values was comparable to their values. The uncertainty in the values for $He^+$ restricted conics and conic events at latitudes greater than 80° is the direct result of too few events. The large uncertainty in the values of $J_{PATH}$ for latitudes less than 65° comes from the comparable number of upflowing and downflowing events found in this latitude range and the large relative uncertainties in the value determined by subtracting numbers of comparable magnitude.

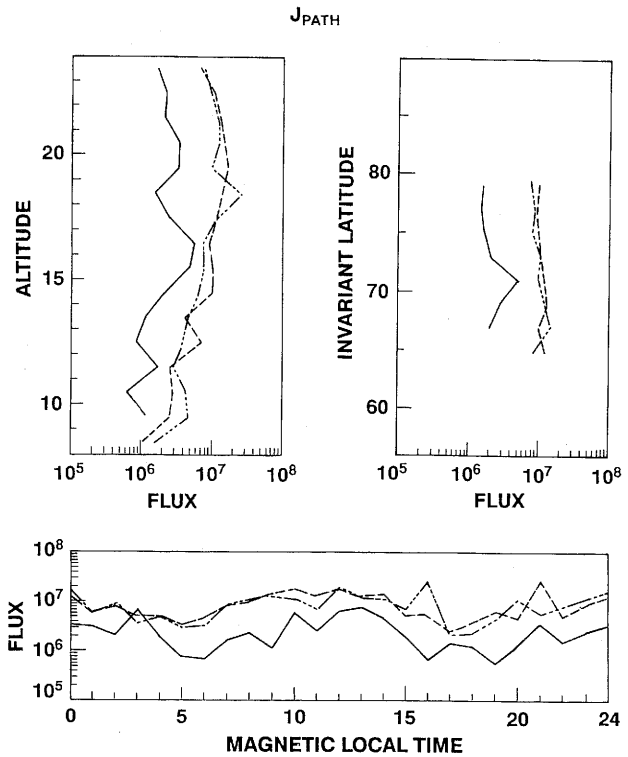


Fig. 13. Distribution in altitude, invariant latitude, and magnetic local time of the average value of $J_{PATH}$ in units of $(cm^2\text{-s-sr-keV})^{-1}$. $J_{PATH}$ is defined by Equations 1 and 5. The format is the same as Figure 12 except only three of the types of ion conic distribution identified by our algorithm are displayed. Key: ... $O^+$ restricted; _ .. _ $O^+$ extended; and ____ He+ restricted.

Figure 13 shows that the upward directed flux associated with restricted and extended $O^+$ events is comparable in all regions of the magnetosphere and that the $He^+$ conic fluxes are, on average ~20% of the $O^+$ fluxes. The altitude distribution shows a steady increase in $J_{PATH}$ from 8,000 to ~17,000 km where it remains more or less constant at a value of $10^7$ $(cm^2\text{-s-sr-keV})^{-1}$. The magnetic local time distribution shows the maximum $J_{PATH}$ values at MLT's near the region of peak occurrence frequency shown in Figure 12. The invariant latitude distribution of $J_{PATH}$ values is constant for $O^+$ conics.

Figure 14 presents the average value of $E_{PATH}$ as a function of altitude, invariant latitude and magnetic local time. A correction similar to that shown in equation 5 to account for the contribution of false positive upflowing conics by using the value determined from the identified downflowing false positive conics has been applied to the data shown in Figure 14. $E_{PATH}$ values for $He^+$ restricted conics, conic events at latitudes greater than 80°, less than 68 °, and altitudes less than 12,000 km are not shown because of the uncertainties in calculating the average value are large. Preliminary analysis shows that the source of the variation in the MLT distribution of $E_{PATH}$ values of $O^+$ extended conics does not come from the statistical uncertainty of the measurement, a more detailed investigation to determine the source of the MLT variation has been undertaken. The working hypothesis for this investigation is that the variation is related to variations in geomagnetic activity at the times the data were acquired.

## DISCUSSION

Above we have presented details of the two dimensional algorithm we have developed to identify and characterize energetic ion conic distributions. We have also compared restricted ion conic distributions identified by the algorithm with the results from earlier morphological studies. In this section we discuss the results we have obtained using our new algorithm.

The data presented in Table 1 and Figures 12-14 present the first detailed results from the application of an improved procedure to automatically identify, classify, and characterize extended energetic ion conic events. We have determined that at altitudes above 15,000 km conic distributions with an extended angular distribution occur more frequently than ion conic distributions with restricted angular distributions. We have determined that extended conic distributions are a non-negligible fraction of the conic distributions found at altitudes above 8,000 km, all invariant latitudes and magnetic local times sampled by the DE -1 spacecraft. We have also assembled some average plasma parameters calculated from the flux images and conic paths in order to learn more about the transverse ion energization processes acting at mid altitudes (8,000 to 25,000 km).

The distribution in space of the occurrence frequency, average flux, $J_{PATH}$, and energy, $E_{PATH}$, for restricted and extended $O^+$ conic distributions have some similarities and differences that place constraints on micro and/or macro physical mechanisms that generate $O^+$ conic distributions. (We defer discussion of the similarities and differences in $He^+$ conic parameters until we have binned them into altitude, magnetic local time, and invariant latitude bins broad

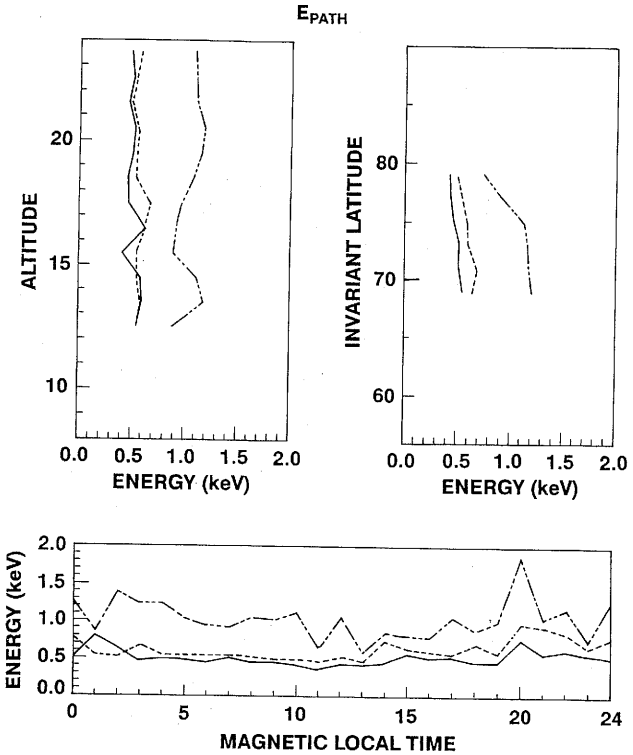


Fig. 14. Distribution in altitude, invariant latitude, and magnetic local time of the average value of $E_{PATH}$ in units of keV. $E_{PATH}$ is defined by Equation 2 and a second equation similar to Equation 5. The format is the same as Figure 12 except only three of the types of ion conic distribution identified by our algorithm are displayed. Key: ... $O^+$ restricted; _ .. _ $O^+$ extended; and ____ He+ restricted.

enough to provide statistically significant samples over the entire volume of space sampled by DE -1.) As noted in the discussion of the data presented in Figure 12 above, the occurrence frequency of $O^+$ restricted and extended conics have almost identical distributions in invariant latitude, slightly different distributions in magnetic local time, and dissimilar distributions in altitude. The peak occurrence frequency at 77° INVL corresponds roughly to the peak of auroral activity in the 6:00 to 12:00 interval where the distribution in magnetic local time is maximum. The occurrence frequency distribution of extended conics has a much stronger altitude dependence than that for restricted conics. The broader distribution of restricted conics in magnetic local time and distinctly different distribution in altitude could arise from several sources including differences in the MLT distributions of the energy sources responsible for formation of the two types of conic. We also note that the increase in the occurrence frequency of extended ion conics with altitude is consistent with their generation by broad band, low frequency waves generated above 25,000 km and transported down

magnetic field lines as discussed by Crew et al. [1990], and André et al. [1990].

The average $J_{PATH}$ values for $O^+$ restricted and extended conics shown in Figure 13 are similar. Two other features of the average $J_{PATH}$ values for $O^+$ restricted and extended conics are remarkable: 1) the independence of the average $J_{PATH}$ value on invariant latitude; and 2) the steady fall off in the average $J_{PATH}$ value at altitudes below 17,000 km. The equality of the average $J_{PATH}$ values for $O^+$ restricted and extended conics and lack of variation in invariant latitude most probably reflects a common ionospheric source population. This is not an unanticipated conclusion. Peterson et al. [1993] used simultaneous observations of $O^+$ ion distributions obtained at two altitudes on auroral magnetic field lines to conclude that multiple heavy ion acceleration processes act on the same field line. The processes include an ionospheric pre-energization mechanism that provides sufficient energy to transport $O^+$ ions with energies in the range 1 - 10 eV to altitudes ~ 5,000 km; and transverse and parallel energization at altitudes above the ionosphere. The steady fall off of the average $O^+$ $J_{PATH}$ values below 17,000 km could be a threshold effect as discussed below.

The average $E_{PATH}$ values for $O^+$ restricted and extended conics have essentially the same distributions in altitude, invariant latitude, and magnetic local time. These distributions have less variations than those for occurrence frequency or $J_{PATH}$. The most remarkable feature of the $E_{PATH}$ data displayed in Figure 14 is that extended $O^+$ conics have an average $E_{PATH}$ value approximately twice that of restricted $O^+$ conic distributions. This difference in $E_{PATH}$ values for $O^+$ restricted and extended conics and their weak variation in altitude, magnetic local time and invariant latitude could be an artifact of the algorithm or of the data. A preliminary investigation of variation in $E_{PATH}$ and the average temperature determined by fits to Equation 4 about their average values showed, in some altitude, invariant latitude, and magnetic time ranges, variations comparable with the average values. Clearly a systematic investigation of the variation of parameters derived from conic paths and flux images must be performed before conclusions based on the data presented in Figure 14 are made. Such a study is planned, but has not yet been performed.

We now return to the the topic of the altitude dependance of $J_{PATH}$ values. the most probable explanation for the slow, steady fall off of average $O^+$ $J_{PATH}$ values below 17,000 km is a threshold effect, where the ion population acquires energy as it goes up the magnetic field line until, on average, at 17,000 km most ion distributions are above the energy threshold of our study. This suggests that there should be an detectable increase in a characteristic energy, such as $E_{PATH}$, as a function of altitude. As noted above there are large variations in $E_{PATH}$ values at fixed altitudes which could mask a systematic increase in $E_{PATH}$ with altitude. No clear altitude dependence of $E_{PATH}$ is detectable in Figure 14.

The data presented above and in recent reports by Peterson et al., [1992], Miyake et al. [1993], and Peterson et al. [1993] provide some new insights into the distribution in altitude of transverse ion acceleration processes. The literature discussing the transverse ion energization mechanisms responsible for generating conic distributions is enormous, too large to review or even briefly summarize here. A good introduction, however, to this literature has been prepared by Klumpar, [1986].

Peterson et al. [1993] used simultaneous observations of $O^+$ ion distributions obtained at two altitudes on auroral magnetic field lines to conclude that multiple heavy ion acceleration processes commonly act on the same field line. Peterson et al. [1992] have examined the altitude dependence of restricted conic distributions presented in Figure 12 and reported the average pitch angle of the restricted conic events as a function of altitude. From these results and a report of a similar study made from data acquired below 10,000 km by the Akebono satellite [Miyake et al. 1993] Peterson et al. [1992] concluded that conic formation by localized, explosive, transverse energization is not the dominate mechanism responsible for producing the energetic conic distributions found above 8,000 km. The data presented in Figures 13 and 14 affirm the conclusion of Peterson et al. [1992] and further show that the upflowing flux associated with energetic conic events has less variation at a given altitude, invariant latitude or magnetic local time than a characteristic energy ($E_{PATH}$) of the distribution.

The picture that emerges from these recent observations is that transverse ion energization occurs in varying degrees at all altitudes above the ionosphere on auroral field lines.

## CONCLUSIONS

We have developed and demonstrated an algorithm to identify and characterize energetic ion conic events and used the algorithm to classify and characterize a very large number of energetic ion conic events. We have noted slight differences in the conic events identified by our two dimensional algorithm and an earlier, one dimensional, algorithm used on the same data.

The data presented here are the first morphological study of the occurrence frequency distribution and average energy and flux associated with extended ion conic events. They show that, at altitudes above 15,000 km, conic distributions with an extended angular distribution occur more frequently than ion conic distributions with restricted angular distri-

butions. We have determined that extended conic distributions are a substantial fraction of the conic distributions found at altitudes above 8,000 km, all invariant latitudes and magnetic local times sampled by the DE -1 spacecraft. These data and other recent reports affirm the conclusion that transverse ion energization occurs in varying degrees at all altitudes above the ionosphere on auroral field lines.

*Acknowledgments.* We gratefully acknowledge helpful discussions with Andrew Yau, Mats André, and Geoff Crew. We thank Daryl Carr for help with assembling the data base. Support was provided by NASA contract NAS5-33032 and the Lockheed Independent Research program.

## REFERENCES

André, Mats, G.B. Crew, W.K. Peterson, A.M. Persoon, C.J. Pollock, and M.J. Engebretson, Ion heating by broadband low-frequency waves in the cusp/cleft, *J. Geophys. Res. 95, 20809*, 1990.

Chang, T., G.B. Crew, N. Hershkowitz, J.R. Jasperse, J.M. Retterer, and J.D. Winningham, Transverse acceleration of oxygen ions by electromagnetic ion cyclotron resonance with broad band left-hand polarization waves, *Geophys. Res. Lott. 13*, 636, 1986.

Crew, G.B., T. Chang, J.M. Retterer, W.K. Peterson, D.A. Gurnett, and R.L. Huff, Ion cyclotron resonance heated conics: Theory and observations, *J. Geophys. Res. 95*, 3959, 1990.

Davis, C., and N. Vaidta, Software for optical archive and retrieval (SOAR), users' guide, National Space Science Data Center, Greenbelt Maryland, *NSSDC/WDC-A-R&S, 89-16,* 1989.

Doherty, M.F., C.M. Bjorklund, W.K. Peterson and H.L. Collin, Automatic detection of mass-resolved ion conics, Lockheed Document Number *IEEE Transactions on Geoscience and Remote Sensing,* 31, 407 1993.

Gorney, D.J., A. Clarke, D. Croley, J.F. Fennell, J. Luhmann, and P.F. Mizera, The distribution of ion beams and conics below 8000 km, J. Geophys. Res. 86, 83, 1981.

Gorney, D.J. Y.T. Chiu, and D.R. Croley, Jr., Trapping of ion conics by downward parallel electric fields, *J. Geophys. Res. 90*, 4205, 1985.

Hoffman, R.A., and Schmerling, E.R., Dynamics Explorer program: An overview, *Space Sci. Instrum. 5,* 345, 1981.

Horwitz, J.L., Velocity filter mechanism for ion bowl distributions (bimodal conics), *J. Geophys. Res. 91*, 4513, 1986.

Klumpar, D.M., W.K. Peterson, and E.G. Shelley, Direct evidence for two-stage (bimodal) acceleration of ionospheric ions, *J. Geophys. Res. 89*, 10779, 1984

Klumpar, D.M., A digest and comprehensive bibliography on transverse auroral ion acceleration, in *Ion Acceleration in the Magnetosphere and Ionosphere,* Tom Chang, Ed., Geophysical Monograph #38, American Geophysical Union, Washington DC. p 389, 1986.

Kondo, T., B.A. Whalen, A.W. Yau, and W.K. Peterson, Statistical analysis of upflowing ion beam and conic distributions at DE -1 altitudes, *J. Geophys. Res. 95*, 12091, 1990.

Miyake, W., T. Mukai, and N. Kaya, On the evolution of ion conics along the field line from Exos -D observations, t*J. Geophys. Res.*, 98, 11127, 1993.

Peterson, W.K., E.G. Shelley, S.A. Boardsen, D.A. Gurnett, B.G. Ledley, M. Sugiura, T.E. Moore, and J.H. Waite, Transverse ion energization and low-frequency plasma waves in the mid-altitude auroral zone: A case study, J. Geophys. Res. 93, 11405, 1988.

Peterson, W.K., H.L. Collin, M.F. Doherty, and C.M. Bjorklund, $O^+$ and $He^+$ restricted and extended (bi-modal) ion conic distributions, Geophys. Res. Lett., 19, 1439, 1992.

Peterson, W.K., A.W. Yau, and B.A. Whalen, Simultaneous observations of $H^+$ and $O^+$ ions at two altitudes by the Akebono and Dynamics Explorer -1 satellites, *J. Geophys. Res.*, 98, 11177 1993.

Sagawa, E., A.W. Yau, B.A. Whalen, and W.K. Peterson, Pitch angle distributions of low-energy ions in the near-Earth magnetosphere, *J. Geophys. Res. 92*, 12241, 1987.

Sharp, R.D., R.G. Johnson, and E.G. Shelley, Observation of an ionospheric acceleration mechanism producing energetic (keV) ions primarily normal to the geomagnetic field direction, *J. Geophys. Res. 82*, 3324, 1977.

Shelley, E.G., D.A. Simpson, T.C. Sanders, E. Hertzberg, H. Balsiger, and A. Ghielmetti, The energetic ion composition spectrometer (EICS) for the Dynamics Explorer -A, *Space Sci. Instrum. 5,* 443, 1981

Temerin, M., Evidence for a large bulk ion conic heating region, *Geophys. Res. Lett. 13*, 1059, 1986.

Thelin, B., B. Aparicio, and R. Lundin, Observations of upflowing ionospheric ions in the mid-altitude cusp/cleft region with the Viking satellite, *J. Geophys. Res. 95*, 5931, 1990.

Yau, A.W., B.A. Whalen, W.K. Peterson, and E.G. Shelley, Distributions of upflowing ionospheric ions in the high-altitude polar cap and auroral ionosphere, *J. Geophys. Res.* 89, 5507, 1984.

---

W.K. Peterson, H.L. Collin, and C.M Bjorklund, Lockheed Palo Alto Research Laboratory, Palo Alto, California 94304.

M.F. Doherty, 913 Laguna Ave., Burlingame, California 94010